Bulg. J. Phys. **44** (2017) 334–344

Density and Isospin Dependence of Spin-Orbit Splittings in N=20 Nuclei within Relativistic Mean-Field Models

G.A. Lalazissis[1], **K. Karakatsanis**[1], **P. Ring**[2], **E. Litvinova**[3,4]
[1]Aristotle University of Thessaloniki, Dept. Physics, GR-54124 Thessaloniki, Greece
[2]Technical University of Munich, Dept. Physics, D-85747 Garching, Germany
[3]Western Michigan University, Dept. Physics, Kalamazoo, MI 49008 USA
[4]MSU, NSCL, East Lancing MI 48824 USA

Received *22 October 2017*

Abstract. An essential ingredient for our understanding of the shell structure in nuclei is the spin-orbit coupling. The fact that, in relativistic mean field (RMF) models of nuclear structure, the large spin-orbit (SO) potential emerges naturally from the form of the the Dirac equation, is one of their most important advantages. Following recent experimental studies, we investigate the size of $2p$- and $1f$-splittings for the isotone chain ^{40}Ca, ^{38}Ar, ^{36}S, and ^{34}Si in the framework of various relativistic density functionals. We compare our results with those of non-relativistic models and with the corresponding experimental data.

PACS codes: 21.60.-n, 21.60.Jz

1 Introduction

A very successful way to study nuclear structure phenomena all over the nuclear chart, are self-consistent mean field models within the density functional framework. In that context, one thinks of nucleons as independent particles inside the nucleus moving under the influnce of various potentials, derived from the density functional [1].

In general, there exist two versions of this theory. The standard are non-relativistic functionals developed first, fifty years ago. The Skyrme type [2] and the Gogny type functionals [3] are the most widely known. In following years relativistic functionals based on the Walecka model [4,5] were also introduced. Their density dependence comes from the non-linear meson coupling included in the model by Boguta and Bodmer [6]. One of the differences between these two versions, is the way the spin-orbit part of the nuclear force is included in

 1310–0157

them. In non-relativistic functionals one needs an extra term whereas in covariant functionals it arises naturally from the Dirac equation. Subsequently, there is a difference in the isospin and density dependence of the effective SO potential between the two types of functionals. In general, it has the form

$$V_{S.O.} = \boldsymbol{W} \cdot (\boldsymbol{p} \times \boldsymbol{\sigma}) \,, \tag{1}$$

where the parameter W entails the isospin and density dependence. In both types of functionals it can be reduced to the following form:

$$\boldsymbol{W}_\tau = W_1 \boldsymbol{\nabla} \rho_\tau + W_2 \boldsymbol{\nabla} \rho_{\tau' \neq \tau}, \tag{2}$$

where τ denotes the isospin value. The ratio W_1/W_2 determines the isospin dependence. In the case of the non-relativistic functionals this has a fixed value equal to 2 [1]. In contrast, in the relativistic functionals this value is close to unity, its value is not fixed but it depends also on the density.

An attempt to set experimental constraints on the spin-orbit term was published recently. In particular, the extreme neutron-to-proton density asymmetry in the case of ^{34}Si, was used. This asymmetry is caused by the bubble structure of ^{34}Si, that was experimentally observed in Ref. [7]. In an earlier experiment by Burgunder *et. al.* [8], it was shown that the corresponding central density depletion causes a large and abrupt reduction in the size of the $2p = 2p_{1/2} - 2p_{3/2}$ spin-orbit splitting. The combination of those two experiments provides a unique method to evaluate the isospin and density dependence of the SO term in various theoretical models.

2 Results

Following the example of the experiment [8] we concentrate our study to the series of $N = 20$ isotones. More specifically, we calculate the single particle energies of the first $1f_{7/2}$, $2p_{3/2}$, $2p_{1/2}$ and $1f_{5/2}$ neutron states. Starting with the nucleus ^{40}Ca with $Z = 20$ protons. Next we go to ^{38}Ar and by removing two more we reach ^{36}S which has its two protons in the $2s_{1/2}$ orbit. The spatial distribution of this wave-function is peaked at the center of the nucleus. Hence, in ^{34}Si where this is an empty state, we have a central depletion in the proton density and the formation of bubble structure.

2.1 Pure mean-field effects

In the first step, we carried out our calculations in the pure mean field level, i.e. without pairing correlations. This gives solely the effect of the relativistic mean field on the spin-orbit splittings.

The results for this case are given in Table 1. In the upper part we show the $f = 1f_{7/2} - 1f_{5/2}$ and $p = 2p_{3/2} - 2p_{1/2}$ energy splittings for each specific

Table 1. Spin-orbit splittings in MeV (left part) and their relative reductions (right part) for f and p neutron states in the case of no pairing.

		^{40}Ca		^{38}Ar		^{36}S		^{34}Si		^{40}Ca $\rightarrow$ ^{36}S		^{36}S $\rightarrow$ ^{34}Si	
	$\frac{W_1}{W_2}$	f	p	f	p	f	p	f	p	f	p	f	p
NL3	1.11	7.21	1.69	6.90	1.77	6.43	1.80	6.08	0.71	11%	-6%	5%	61%
DD-ME2	1.07	7.40	1.71	7.04	1.72	6.52	1.65	6.12	0.87	12%	3%	6%	47%
DD-PC1	1.07	7.83	1.77	7.57	1.74	7.12	1.64	6.61	0.88	9%	8%	7%	46%
Exp.		6.98	1.66			5.61	1.99	5.5	1.13	20%	-20%	2%	43%

functional and for each of the nuclei ^{40}Ca, ^{38}Ar, ^{36}S, and ^{34}Si. In the lower part we present the relative reduction of the f and p splittings again for every functional, first as we move from ^{40}Ca to ^{36}S and then as we go from ^{36}S to ^{34}Si. We also show in the last row the experimental values of the splittings and the reductions for ^{40}Ca [9], ^{36}S [11], and ^{34}Si [8]. Finally, in the first second column we show the value of the ratio W_1/W_2 for each functional as it is calculated in Ref. [10]

These resuts along with those for the non-relativistic SLy5 and D1S models from Ref. [12] again in the pure mean-field scheme with no pairing correlations included, are given schematically in Figure 1. For all the models we plot the evolution of the p and the f spin-orbit splittings as a function of the mass number A.

Concentrating in the f splittings we see a gradual reduction of about 0.3-0.4 MeV moving form one nucleus to the next. Another way to confirm this, is by looking at the curves that show the evolution of the f-splitting in Figure 1and recognis-

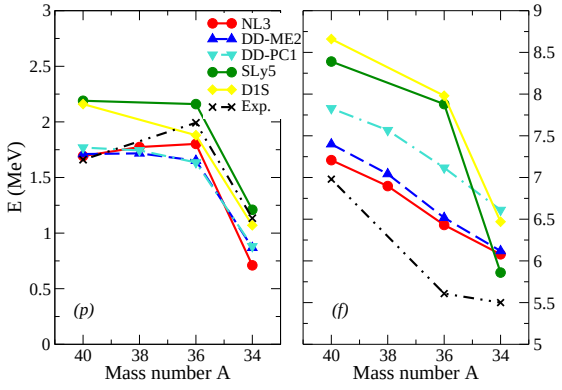

Figure 1. (color online) Evolution of spin-orbit splittings for the neutron levels p (left panel) and f (right panel) with respect to the mass number A, without pairing.

ing the same slope for the different functionals. The total relative reduction is between 15-19% and around 5-7% at each step.

Contrary to the f-splittings, the p splittings stay practically constant. Only in the transition from ^{36}S to ^{34}Si we discover the large reduction of the p splittings at the order of 40% to 60%. This is in agreement with experimental results, as a qualitative picture. However, the absolute size of the p-splitting in ^{34}Si for most of our models is smaller than the respective experimental value. This causes an even larger relative reduction than what we expect.

The comparison between relativistic and non-relativistic models shows also significant differences. In general the sizes of the splittings in all the relativistic models are smaller than the respective splittings in non-relativistic models. More specifically, in the nuclei first three nuclei, where the proton density has the normal profile, i.e. no central depletion, the f-splittings are 1-2 MeV larger and the p-splittings are about 0.5 MeV larger in the non-relativistic case. In the bubble nucleus ^{34}Si, the f-splittings have the same size for both kinds of functionals. This is because of the bigger reduction that appears in the non-relativistic case which is not present in the relativistic models. However, the p-splittings are comparatively smaller for all the relativistic functionals. Thus, the relative reduction of the p-splitting between ^{36}S and ^{34}Si, is larger for most of the relativistic models than the same reduction for non-relativistic models.

2.2 The effect of pairing correlations

In the second step, the same calculations are repeated with pairing correlations now included, in the Relativistic Hartree Bogoliubov (RHB) framework. In particular, for the short range correlations the TMR separable pairing force of Ref. [13] is used.

Within that framework, the smoothening of the bubble in ^{34}Si, because of pairing correlations, was theoretically predicted in Ref. [14]. Therefore, a change in the size of the SO splittings is expected. Subsequently, we introduce pairing correlations in the proton subsystem and evaluate again the single-particle energies of the same neutron states as before. Furthermore, within the RHB, the occupancy of each state is determined by the strength of the pairing force and is calculated self-consistently, using the concept of quasiparticles. Hence, the occupation probabilities of the proton $2s_{1/2}$ state for ^{36}S and ^{34}Si, are also calculated and compared with the experimentally deduced value in Ref. [7].

The SO splittings and the respective reductions found in these calculations are shown in Table 2. Additionally, in Figure 2 a schematic representation of the evolution of SO splittings is shown for all the forces with respect to the mass number.

Comparing the previous results with those including pairing, one sees a similar qualitative picture. That is, a gradual reduction of the f-splittings with the de-

Table 2. Same as Table 1 but for the case of TMR pairing.

	^{40}Ca		^{38}Ar		^{36}S		^{34}Si		^{40}Ca $\rightarrow$ ^{36}S		^{36}S $\rightarrow$ ^{34}Si	
Splitting	f	p	f	p	f	p	f	p	f	p	f	p
NL3	7.21	1.69	6.92	1.64	6.46	1.68	5.94	0.80	10%	1%	8%	53%
DD-ME2	7.40	1.71	7.08	1.64	6.55	1.57	6.00	0.94	11%	8%	8%	40%
DD-PC1	7.83	1.77	7.58	1.67	7.14	1.56	6.52	0.96	9%	12%	9%	39%
Exp.	6.98	1.66			5.61	1.99	5.5	1.13	20%	-20%	2%	43%

crease in neutron number. No change in the size of the p-splittings for the three first nuclei followed by a dramatic reduction for the last bubble nucleus.

Looking at the results more closely one observes the following quantitave changes. In ^{38}Ar and ^{36}S the size of the f-splittings is increased and the size of p-splittings is decreased by the inclusion of pairing. This specific change is more pronounced for the p-splittings for ^{36}S and for the f-splittings for ^{38}Ar. In the ^{34}Si nucleus we get the opposite picture with smaller f-splittings and larger p-splittings, in the order of magnitude of 0.1MeV. In total, these changes correct for the enhanced effect of the bubble structure and the relatively large reduction of the p-splitting of the pure mean field case.

In addition, the calculation of the occupation probability of the $2s_{1/2}$ proton state in ^{36}S and ^{34}Si, see Table 3, provides a better understanding of the way pairing causes the changes in the SO splittings mentioned above. In ^{38}Ar, pairing affects mostly the *1d* proton orbit with its two last 2 protons in the $1d_{3/2}$ state. Here the greater surface diffusion means that the spin-orbit force overlaps more with the f neutron states causing bigger corresponding splittings. In the ^{36}S pairing influences the central densities reducing the size of the peak with a tendency to flatten it out. This can also be seen by the reduced occupancy of the $2s_{1/2}$ proton state which is now smaller than 2. This creates a less attractive SO force around

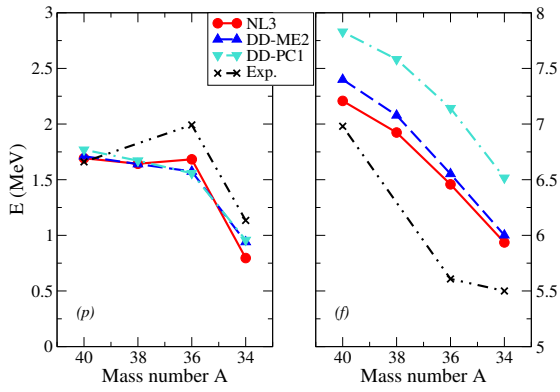

Figure 2. (color online) Same as in Figure 3 but with TMR pairing.

Table 3. Occupation probabilities of the $2s_{1/2}$ proton state in ^{36}S and ^{34}Si for the TMR pairing force.

	^{36}S	^{34}Si	$\Delta(2S_{1/2})$
NL3	1.83	0.20	1.62
DD-ME2	1.79	0.23	1.57
DD-PC1	1.77	0.30	1.47
Exp. [7]	1.64	0.17	1.56

the center and so the splittings of the neutron p states appear somewhat smaller. In the ^{34}Si pairing correlations correspond to an occupation probability of the $2s_{1/2}$ state in the proton part with a small finite value, rather than being zero, as it is in the pure mean field case. This is why the central dimple in proton density tends to flatten out as it was observed in Ref. [14]. The impact on the *p*-splittings is an increase by about 0.1 MeV. This is caused by the increasing occupancy of the previously empty $2s_{1/2}$ proton state, as shown in Table 3. In the end, the relative reduction of the size of the *p* SO splitting between the two nuclei is described more accurately with the inclusion of pairing correlations.

2.3 Extensions: Tensor forces and particle-vibration coupling

In the final section of our investigation the standard formulation of the covariant density functional models is modified in two ways. The first way, which remains at the mean field level, includes an explicit tensor term in the dynamics of the model. The second way goes beyond the mean field by including correlations of low lying surface modes with single particle states.

2.3.1 The effect of the tensor force

Conventional calculations with covariant density functionals stay at the Hartree level, i.e. they don't include exchange terms in the effective potentials. However, the tensor part of the nuclear force plays an essential role in the description of several nuclear properties. In our case it affects the single particle structure [15–17]. The general rule is that the effective tensor force is attractive between nucleons of different kind that occupy states with antiparallel spin and vice versa. Therefore, it is interesting to examine, whether the explicit inclusion of the tensor force in the specific case of the bubble nucleus ^{34}Si changes the size of the SO splittings and the accompanying reduction. Subsequently, we use a modified functional, the NL3RHF0.5 with an extra term, corresponding to the one pion exchange interaction, that produces the tensor part of the force [17]. The parameters of this specific functional have been adjusted to finite nuclei after choosing the coupling constant of the pion exchange to be half of the observed coupling constant in the πN interaction in free space.

In Table 4 we compare the specific functional NL3RHF0.5 with the calculations of NL3 in the Hartree level and to those of non-relativistic Skyrme and Gogny interactions SLy5$_{T-2013}$ and D1ST$_{2c-2013}$. These are modified versions of the functionals SLy5 and D1S, where tensor terms have been included and were adjusted together with the spin-orbit parameters. Details are given in Ref. [12].

Table 4. Spin-orbit splittings of f and p neutron states (left part) and relative reductions (right part), for the case of tensor forces. For comparison we also show the results from Ref. [12].

	^{40}Ca		^{36}S		^{34}Si		^{40}Ca $\rightarrow$ ^{36}S		^{36}S $\rightarrow$ ^{34}Si	
Splitting	f	p	f	p	f	p	f	p	f	p
NL3	7.21	1.69	6.44	1.68	5.56	0.74	10%	1%	14%	56%
NL3RHF0.5	7.87	1.74	5.80	1.64	5.12	0.66	26%	14%	12%	60%
SLy5$_{T-2013}$	6.77	1.76	5.53	1.07	4.41	0.61	18%	39%	20%	43%
D1ST$_{2c-2013}$	6.90	1.73	5.65	1.26	4.75	0.73	18%	27%	16%	42%
Exp.	6.98	1.66	5.61	1.99	5.5	1.13	20%	-20%	2%	43%

The most obvious difference with the previous calculations is that in the present case of NL3RH0.5 the f splitting is more rapidly reduced as we move from ^{40}Ca to ^{38}Ar to ^{36}S. This shows that the tensor affects mostly the size of the f-splitting, suggesting that the reduction we observe in the p-splitting is mainly a SO effect. This result can be interpreted by the gradual removal of protons from certain orbits and the alternating action of the tensor force on the same f and p neutron states, obeying the general rule described above.

Pairing correlations were also included in the calculations with the one pion exchange functional, in the frozen gap scheme. The measured occupancy is now 0.18 for the proton $2s_{1/2}$ state in the nucleus ^{34}Si. Compared with the 0.10 of the conventional NL3 plus pairing result, this larger value in combination with the smaller size of the p splitting which reduced from 0.74 MeV to 0.66 MeV, implies that the inclusion of explicit tensor forces is opposite of the effect of pairing.

2.3.2 The effect of particle vibration coupling

In order to take into account into account interaction of the particles with low lying vibrations we use the time-dependent density functional theory [18]. Staying in the small-amplitude limit and applying the linear-response theory one can determine the time dependent of the system's self-energy. This approach is known as the random-phase approximation (RPA). One starts from a static solution of DFT and permits around this solution small amplitude vibrations. The calculation of linear superpositions of *ph* excitations that describe surface phonons i.e. surface excitations is done by the diagonalization of the RPA matrix. The second derivative of the energy density functional with respect to the density give the

interaction between the *ph* pairs.

$$V(\mathbf{r}_1, \mathbf{r}_2) = \frac{\delta^2 E[\rho]}{\delta\rho(\mathbf{r}_1)\delta\rho(\mathbf{r}_2)}. \tag{3}$$

In the end one gets the harmonic vibrations $|\mu\rangle$ of the system with the corresponding eigen-frequencies Ω_μ and the transition densities $\delta\rho^\mu_{12} = \langle\mu|a^\dagger_2 a_1|0\rangle$. Following that, one needs to go back to the static mean-field self energy and add terms that describe the single-particle motion under the influence of these vibrations. These terms are then energy dependent and the coupling is given by the vertices

$$\gamma^\mu_{12} = \sum_{34}\langle 14|V|23\rangle\delta\rho^\mu_{34}, \tag{4}$$

where $\langle 14|V|23\rangle$ are the matrix elements of the interaction (3) and $\delta\rho^\mu_{34}$ are the transition densities of the corresponding phonons.

The important modification induced by the particle vibration coupling scheme [19,20] on the usual mean field-independent particle picture, is the fragmentation of the single particle states. Usually the major contribution goes to the fragment with the lower energy which is also shifted in lower energy relative to the mean field value. This is more relevant for states near the Fermi surface which interact more with surface vibrations. The great advantage here is that one can compare directly that major component of each state with the experimental one, in particular from Ref. [8]. For our calculations we used the density functional NL3* [21] for the static solutions and a constant pairing gap of $\Delta = 2$ MeV. Non-spin-flip phonons μ with natural parities, angular momenta $L_\mu \leq 6$, and frequencies $\Omega^\mu \leq 20$ MeV have been included into the self-energy.

In Table 5, we compare the calculated values of the *f* and *p* splittings between the major fragments for the nuclei ^{36} and ^{34}Si with the respective experimental values. Additionally, we see in the lower part of the table that the experimental reduction which is 43% fo the *p* neutron states is described rather accurately by the PVC calculations.

In Figure 3 we concentrate on the positions of the major fragments of the neutron states $2p_{1/2}$, $2p_{3/2}$ and $1f_{5/2}$ with respect to the $1f_{7/2}$ which is set to zero. In particular, we show in the following order first the results from Ref. [8], then

Table 5. Comparison between the spin-orbit splittings (left part) and their relative reductions (right part) of the major fragments from PVC with the corresponding experimental results.

	^{36}S		^{34}Si		^{36}S $\rightarrow$ ^{34}Si	
Splitting	*f*	*p*	*f*	*p*	*f*	*p*
NL3* with PVC	6.3	2.28	5.28	1.4	16%	39%
Exp.	5.61	1.99	5.5	1.13	2%	43%

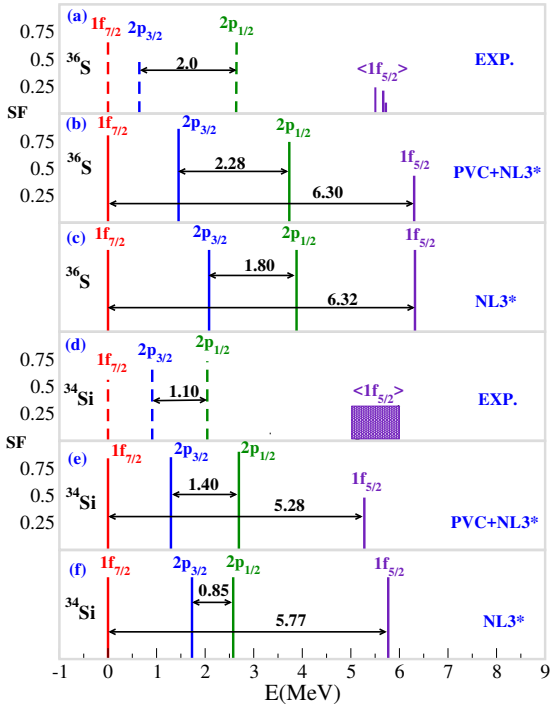

Figure 3. (color online) Distribution of the major fragments of the single particle strengths of ^{37}S (panel (a)) and ^{35}Si (panel (d)) as given in Ref. [8] and the same distribution calculated with PVC for the force NL3* (panels (b) and (e)). Panels (c) and (f) show results obtained without particle vibrational coupling using the same density functional.

from PVC+NL3*, and lastly from standard mean field. For both ^{36}S and ^{34}Si nuclei, the position of the f state and the size of the corresponding splitting is described rather good. The coupling of particles to vibrations changes only slightly the size of their splitting. On the other hand, it moves the states $2p_{3/2}$ and $2p_{1/2}$ closer to the reference state $1f_{7/2}$. This change is more pronounced for the $2p_{3/2}$ which is closer to the Fermi surface. In total, in both nuclei the size of the SO-splitting between those states increases with PVC.

3 Conclusions

Summarizing our results we can conclude to the following findings. The application of several covariant density functionals in the RMF framework, reproduces the general qualitative picture observed experimentally. Concentrating on the size of the neutron $2p_{3/2} - 2p_{1/2}$ SO splitting one gets a significantly smaller size in ^{34}Si than the one in ^{36}S. In the first step of the pure mean field cal-

culations the effect of the bubble in the proton density of ^{34}Si, resulted in an enhancement of the reduction relative to the experiment and to non-relativistic models. This enhancement is corrected in the next step with the consideration of pairing correlations in the proton subsystem of the nuclei.

Two specific extensions were also considered, in order to examine the behaviour of the SO splittings. The first was the explicit consideration of the tensor force induced by the pion exchange. The second was particle-vibration coupling which goes beyond the simple mean field level. Our results, suggest that the effect of the tensor, though small, opposes the effect of pairing. The decrease in size of the *f* splitting, as we move from ^{40}Ca to ^{34}Si, is enhanced. At the same time, the *p*-splitting is slightly smaller for all nuclei and so the relative reduction is unchanged, indicating that the observed experimental reduction is truly a SO effect. Finally, we were able to compare directly with the experimental results with the extension of PVC. This particular scheme proved to be very accurate for the description of the specific reduction of the *p* SO splitting in the bubble nucleus.

Acknowledgments

For the participation at SDANCA G.A. Lalazissis acknowledges support from the Bulgarian fund under contract No DFNI-E02/6. This research was funded by the Greek State Scholarship Foundation (IKY), through the program "IKY Fellowships of excellence for postgraduate studies in Greece-SIEMENS program", by the DFG cluster of excellence "Origin and Structure of the Universe" (www.universe-cluster.de), and by US-NSF grant PHY-1404343.

References

[1] M. Bender, P.-H. Heenen, and P.-G. Reinhard (2003) *Rev. Mod. Phys*. **75** 121.
[2] D. Vautherin and D.M. Brink (1972) *Phys. Rev. C* **5** 626.
[3] J. Dechargé and D. Gogny (1980) *Phys. Rev. C* **21** 1568.
[4] J.D. Walecka (1974) *Ann. Phys. (N.Y.)* **83** 491.
[5] B.D. Serot and J.D. Walecka (1986) *Adv. Nucl. Phys.* **16** 1.
[6] J. Boguta and A.R. Bodmer (1977) *Nucl. Phys. A* **292** 413.
[7] A. Mutschler, A. Lemasson, O. Sorlin, D. Bazin, C. Borcea, R. Borcea, Z. Dombradi, J.-P. Ebran, A. Gade, H. Iwasaki, E. Khan, A. Lepailleur, F. Recchia, T. Roger, F. Rotaru, D. Sohler, M. Stanoiu, S.R. Stroberg, J.A. Tostevin, M. Vandebrouck, D. Weisshaar, and K. Wimmer (2016) *Nature Phys.* **13** 152-156.
[8] G. Burgunder, O. Sorlin, F. Nowacki, S. Giron, F. Hammache, M. Moukaddam, N. de Séréville, D. Beaumel, L. Càceres, E. Clément, G. Duchêne, J.P. Ebran, B. Fernandez-Dominguez, F. Flavigny, S. Franchoo, J. Gibelin, A. Gillibert, S. Grévy, J. Guillot, A. Lepailleur, I. Matea, A. Matta, L. Nalpas, A. Obertelli, T. Otsuka, J. Pancin, A. Poves, R. Raabe, J.A. Scarpaci, I. Stefan, C. Stodel, T. Suzuki, and J.C. Thomas (2014) *Phys. Rev. Lett.* **112** 042502.

[9] Y. Uozumi, N. Kikuzawa, T. Sakae, M. Matoba, K. Kinoshita, S. Sajima, H. Ijiri, N. Koori, M. Nakano, and T. Maki (1994) *Phys. Rev. C* **50** 263.

[10] J.P. Ebran, A. Mutschler, E. Khan, and D. Vretenar (2016) *Phys. Rev. C* **94** 024304.

[11] G. Eckle, H. Kader, H. Clement, F. Eckle, F. Merz, R. Hertenberger, H. Maier, P. Schiemenz, and G. Graw (1989) *Nucl. Phys. A* **491** 205.

[12] M. Grasso and M. Anguiano (2015) *Phys. Rev. C* **92** 054316.

[13] Y. Tian, Z.Y. Ma, and P. Ring (2009) *Phys. Lett. B* **676** 44.

[14] M. Grasso, L. Gaudefroy, E. Khan, T. Niksic, J. Piekarewicz, O. Sorlin, N.V. Giai, and D. Vretenar (2009) *Phys. Rev. C* **79** 034318.

[15] T. Otsuka, T. Suzuki, R. Fujimoto, H. Grawe, and Y. Akaishi (2005) *Phys. Rev. Lett.* **95** 232502.

[16] T. Otsuka, T. Matsuo, and D. Abe (2006) *Phys. Rev. Lett.* **97** 162501.

[17] G.A. Lalazissis, S. Karatzikos, M. Serra, T. Otsuka, and P. Ring (2009) *Phys. Rev. C* **80** 041301.

[18] M.A.L. Marques, C.A. Ullrich, F. Nogueira, A. Rubio, K. Burke, and E.K. U.G. (Eds.) (2006) "*Time-Dependent Density Functional Theory*", Springer, Heidelberg.

[19] E. Litvinova, P. Ring, and V.I. Tselyaev (2008) *Phys. Rev. C* **78** 014312.

[20] E. Litvinova (2012) *Phys. Rev. C* **85** 021303(R).

[21] G.A. Lalazissis, S. Karatzikos, R. Fossion, D. Peña Arteaga, A.V. Afanasjev, and P. Ring (2009) *Phys. Lett. B* **671** 36.